J Mater Sci: Mater Med (2011) 22:2261–2271
DOI 10.1007/s10856-011-4418-0

Electrophoretic deposition of porous CaO–MgO–SiO_2 glass–ceramic coatings with B_2O_3 as additive on Ti–6Al–4V alloy

Wei Zhang · Xianchun Chen · Xiaoming Liao · Zhongbing Huang · Xiuli Dan · Guangfu Yin

Received: 31 January 2011 / Accepted: 6 August 2011 / Published online: 21 August 2011

Abstract The sub-micron glass–ceramic powders in CaO–MgO–SiO_2 system with 10 wt% B_2O_3 additive were synthesized by sol–gel process. Then bioactive porous CaO–MgO–SiO_2 glass–ceramic coatings on Ti–6Al–4V alloy substrates were fabricated using electrophoretic deposition (EPD) technique. After being calcined at 850°C, the above coatings with thickness of 10–150 μm were uniform and crack-free, possessing porous structure with sub-micron and micron size connected pores. Ethanol was employed as the most suitable solvent to prepare the suspension for EPD. The coating porous appearance and porosity distribution could be controlled by adjusting the suspension concentration, applied voltage and deposition time. The heat-treated coatings possessed high crystalline and was mainly composed of diopside, akermanite, merwinite, calcium silicate and calcium borate silicate. Bonelike apatite was formed on the coatings after 7 days of soaking in simulated body fluid (SBF). The bonding strength of the coatings was needed to be further improved.

1 Introduction

Titanium alloys have been widely used as materials for medical applications, especially in load bearing bone restoration and orthopaedics owing to their superior mechanical properties and excellent biocompatibility. However, metallic implants are bioinert, which only can attach to the bone through mechanical interlocking, but not osseointegrating. The unstable integrations are prone to induce failures of implants. An established method to improve tissue adhesion to implant surfaces and hence to provide better implant fixation is to coat the substrates with bioactive inorganic materials, such as glasses, glass–ceramics and ceramics. Hydroxyapatite (HA) coatings on titanium alloys generate significant interests [1–5], especially plasma sprayed HA coatings, because HA is chemically and structurally equivalent to the mineral phase in bones and is thereby biocompatible, bioactive and capable of chemical bonding with surrounding bones. The HA coatings, however, suffer from low bonding strength, since the coefficient of thermal expansion (CTE) of HA differs largely from that of titanium or its alloys, which leads to considerable stress on the interface during preparation process, cooling from high temperature. Thus, it is necessary to synthesize a material possessing matchable CTE with titanium alloy substrate.

Some of the glass–ceramics based on CaO-MgO-SiO_2 system have also been regarded as potential candidates for biomedical applications in recent years. In this system, the probable crystalline phases such as diopside ($CaMgSi_2O_6$), akermanite ($Ca_2MgSi_2O_7$), wollastonite ($CaSiO_3$), merwinite ($Ca_3MgSi_2O_8$), and dicalcium silicate (Ca_2SiO_4), have been thoroughly investigated, showing that they possessed good mechanical, no cytotoxicity, osseointegration and biocompatible properties [6–14]. In addition, the CTE of these components was much closer to that of Ti–6Al–4V alloy ($10.3 \times 10^{-6}°C^{-1}$) [15], ranging from $8.1 \times 10^{-6}°C^{-1}$ to $10.76 \times 10^{-6}°C^{-1}$ [14, 16–19], while the CTE of HA was $13.4 \times 10^{-6}°C^{-1}$ [15]. Weichang Xue et al. [14] prepared diopside coatings on Ti–6Al–4V alloy substrates using an atmospheric plasma spray system, and found that the bonding strength of the coating was higher than that of plasma sprayed HA coating on titanium alloy

W. Zhang · X. Chen · X. Liao · Z. Huang · X. Dan · G. Yin (✉)
College of Materials Science and Engineering, Sichuan University, Chengdu 610064, People's Republic of China
e-mail: nic0700@scu.edu.cn

substrate. Glass–ceramic coatings based on CaO–MgO–SiO_2 system, therefore, have been accepted as a potential substitute for HA coatings on titanium alloys.

Different coating techniques have been developed to produce inorganic coatings on metallic substrates, including plasma spray, sol–gel, enamelling, electrophoretic deposition (EPD), and so on [1, 2, 20–25]. The EPD technique possessed the advantages of high versatility of its use with different materials and their combinations, its cost-effectiveness requiring simple apparatus, the deposition conditions of room temperature, short formation time and little restriction on the substrate shape [20]. In particular, compared with other coating techniques, the EPD process could produce uniform coating on substrates of heterogeneous structure and complex shape. In addition, despite being a wet process, EPD offered easy control of the thickness and morphology of a deposited film through simple adjustment of the deposition time and applied voltage. Hence, it has been widely used in the processing of advanced ceramic materials and coatings, and recently gained increasing interests both in academia and industrial sector. Nevertheless, until now there have been few studies on the CaO–MgO–SiO_2 ternary system coating by EPD [26], and different powders need different suspension systems and EPD conditions. Consequently, this study was to find the optimal conditions to prepare glass–ceramic coatings of CaO–MgO–SiO_2 system on Ti–6Al–4V alloy substrates using EPD method.

In addition, earlier studies demonstrated that B_2O_3 played an important role in lowering the melting point of the glass–ceramics as well as in enhancing sinterability [17]. In this study, accordingly, glass–ceramic powders with nominal composition of $2CaO–MgO–2SiO_2$ and 10 wt% B_2O_3 additive were synthesized by sol–gel method. The results showed that the sintering temperature of the powders with 10 wt% B_2O_3 was decreased to 850–900°C, in which temperature range the phase transition of Ti–6Al–4V alloy could not take place. This study focused on the synthesis of glass–ceramic powders, preparation of suspension and optimization of conditions involving deposition time, suspension concentration and applied voltage during EPD.

2 Materials and experimental procedure

2.1 Synthesis of glass–ceramic powder

The glass–ceramic powders were synthesized by sol–gel process using traethyl orthosilicate ($Si(OC_2H_5)_4$, TEOS), magnesium nitrate hexahydrate ($Mg(NO_3)_2{\cdot}6H_2O$), calcium nitrate tetrahydrate ($Ca(NO_3)_2{\cdot}4H_2O$) and Boric acid (H_3BO_3) as raw materials.

First of all, TEOS was mixed with water (mol ratio: $TEOS:H_2O = 1:4$) in a breaker using HNO_3 to adjust the solution pH value to 2.0 and hydrolyzed under vigorous stirring in a hot-stirrer at 50°C for 30 min afterward, while $Mg(NO_3)_2{\cdot}6H_2O$, $(Ca(NO_3)_2{\cdot}4H_2O$ and H_3BO_3(mol ratio: $TEOS:Ca(NO_3)_2{\cdot}4H_2O:Mg(NO_3)_2{\cdot}6H_2O:H_3BO_3 = 2:2:1:0.43$) were dissolved in water. After the hydrolysis of the TEOS was completed, the mixed solution of $Mg(NO_3)_2{\cdot}6H_2O$, $(Ca(NO_3)_2{\cdot}4H_2O$ and H_3BO_3 was added slowly into the above mixture. After the reactants were stirred at 50°C for 2 h, the transparent sol was formed. The sol was aged at room temperature for 24 h transforming into gel and followed by being dried at 80°C for 24 h. The dried gel was ground and then calcined at 650°C for 2 h in an air furnace to eliminate residual water and nitrates. The powder was ground again in an agate mortar for 10 h.

2.2 Electrophoretic deposition

The Ti–6Al–4V plates (10 mm × 10 mm × 1 mm) were sequentially polished using 120, 400, 600, 800 and 1000 grit emery papers and cleaned with running distilled water, acetone and ethanol in turn. Afterwards, the samples were eroded in 10% (vol%) hydrofluoric acid solution for 30 s and cleaned with distilled water. The solvents for suspension were chosen from ethanol, water, acetic acid, isopropanol and ethanol (90% v/v) versus water by testing zeta potential. Then suspensions for electrophoretic experiments were prepared by adding glass–ceramic powders in ethanol (99.86%). All suspensions were stirred for 30 min and dispersed ultrasonically for 30 min in an ultrasonic bath to ensure a good dispersion of the particles. The concentrations of glass–ceramic powders in the suspensions were 10, 20, 40 g/l. A platinum foil of 10 mm × 15 mm × 0.3 mm was used as the anode and the Ti–6Al–4V substrate was used as the cathode. The distance between the two electrodes was 1 cm. Constant voltage of 10, 20, 40, 60 and 80 V were applied for 30–300 s using a dc power supply (JUNYI JY600, China) between the substrate and the counter electrode, respectively. The obtained coatings were calcined in argon at 850°C for 3 h, with a heating-up rate of 5°C/min.

2.3 Soaking the Ti alloys/glass–ceramic coating in simulated body fluid (SBF)

After being ultrasonically washed in acetone and rinsed in deionized water, the Ti alloys/glass–ceramic coating were soaked in SBF (pH = 7.40) at 37°C for 7 days. The ratio of the surface of specimens to the volume of the SBF solution was 0.05 cm^2/ml. The solution was prepared according to the procedure described by Kokubo [27].

2.4 Method for testing

Zeta potential measurements were tested using a zeta potential analyzer (Malvern Instruments Mastersizer). The surface morphology and the coating thickness were detected by scanning electron microscopies (SEM, JEOL-5900, Japan; TM-1000, Japan). The current was measured with a multimeter. The thermal properties of the glass–ceramic powders were characterized using a thermo gravimetry (TG, NETZSCH STA 49C, Germany) and DSC (DSC, NETZSCH STA 49C, Germany). The crystal structure was examined using an X-ray diffractometer (XRD, X'PERT, Holland). The bond strengths of the coatings on the Ti alloy substrates were evaluated using a universal testing machine (SHIMADZU AG-X, Japan) through the tensile test for five specimens per group. The coatings on the substrates were attached to the metal rod ($\Phi = 7$ mm) with epoxy adhesive (BLUESTAR DG-3S, China). After gluing the metal rods to the sample surfaces, the epoxy adhesive was hardened at 60°C for 2 h. The tensile load was applied at a constant speed of 1 mm/min.

3 Results and discussion

3.1 Glass–ceramic powders

The XRD pattern of the multiphase glass–ceramic powders calcined at 650°C is shown in Fig. 1. The peaks of calcium silicate (Ca_3SiO_5), diopside ($CaMg(SiO_3)_2$), merwinite ($Ca_3Mg(SiO_4)_2$), boron oxide(B_2O_3), calciborite (CaB_2O_4) and other uncrystalline matter were detected by XRD. The relative crystallinity was approximately 33.11%. The low crystallinity was beneficial for sintering of the coating during the heat treatment. The SEM images of the synthesized glass–ceramic powders are displayed in Fig. 2. The particles were spherical with the size of 0.2 to 1.5 μm. Each spherical particle consisted of a great number of agglomerate 20–50 nm particles, which were conducive to decrease the sintering temperature. The particles of these sizes were suitable for electrophoretic deposition according to the report [20].

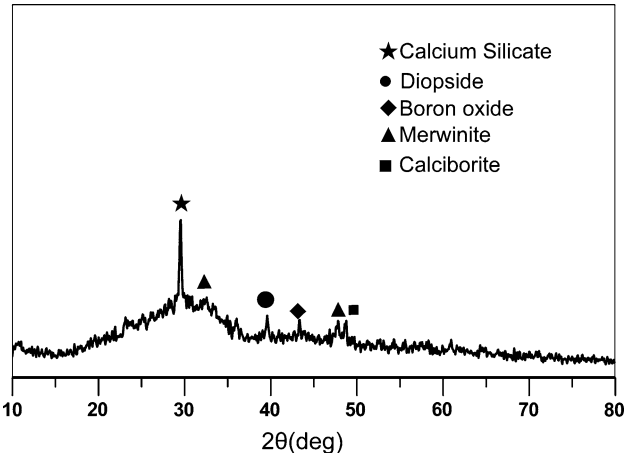

Fig. 1 XRD pattern of the glass–ceramic powders calcined at 650°C for 2 h

3.2 The selection of solvent for suspension preparation

The zeta potential of the suspension is a key factor in the electrophoretic deposition process. It was imperative to achieve a high and uniform surface charge of the suspended particles. It played a role in: (i) stabilization of the suspension that was determined by the intensity of repulsive interaction between particles, (ii) determining the direction and migration velocity of particle during EPD. The zeta potential was determined by the powder surface charge, solvent property and charging additive; accordingly the suspension concentration hardly influenced on zeta potential [20]. The zeta potentials of the suspension in different solvents with 10 g/l suspension concentration are showed in Fig. 3. The powders in water were negatively charged and in n-butanol, acetic acid, ethanol and isopropanol were positively charged. In this study, the titanium alloy substrate should play as cathode, because the anodic oxidization would occur on the surface of the titanium alloy substrate if it was used as anode. Hence, it was required that the powders in suspension were positive and they could move to the titanium alloy substrates as the cathode. Consequently, the negative powders in water were not applicable. Among the other four solvents, the powders in ethanol and acetic acid possessed relatively high Zeta potential, which was beneficial for EPD. However, there were little powders deposited on the substrate in acetic acid. Laxmidhar Besra found that the suitable dielectric constant of solvent was in the range of 12–25 [20]. If the dielectric constant was too low, the deposition failed due to insufficient dissociative powders. The dielectric constant of acetic acid was 6.13 that was too low for EPD [28], which should be responsible for the deposition failure, while the dielectric constant of ethanol was 24.55 [29]. Besides, suspension in ethanol was stable and dispersed with low sedimentation velocity. Therefore, ethanol was the most suitable solvent for the suspension among the five solvents, attributed to the high zeta potential, proper dielectric constant and low sedimentation rate velocity.

3.3 Electrophoretic deposition process

Hamaker described the correlation of the amount of deposited particles during EPD and different influencing parameters through the following equation [30]:

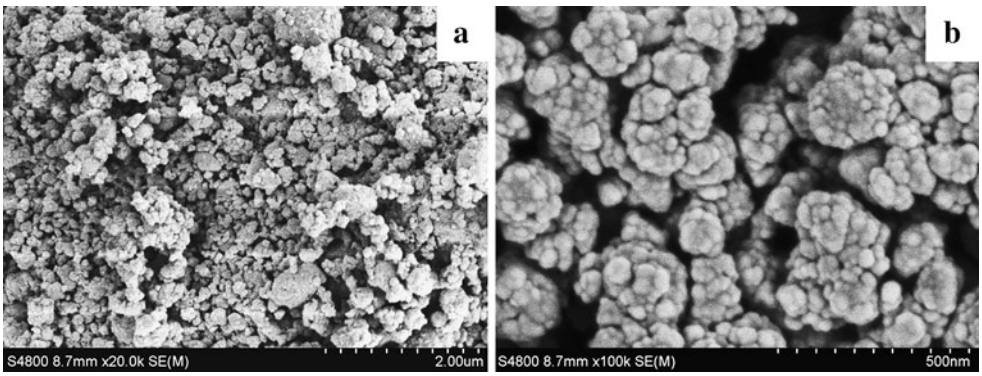

Fig. 2 SEM images of the synthesized glass–ceramic powders calcined at 650°C for 2 h. **a** low magnification; **b** high magnification

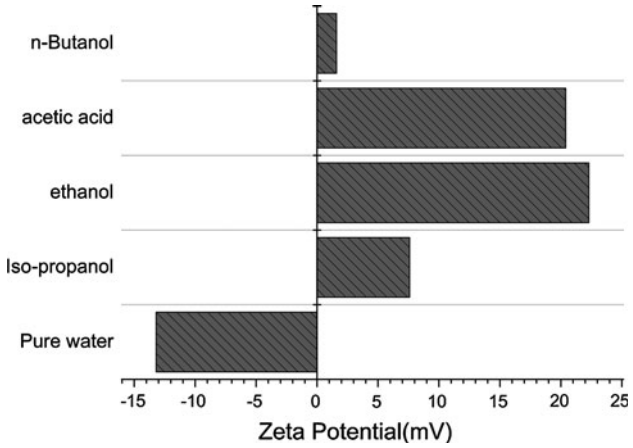

Fig. 3 Zeta potentials of the suspensions in different solvents with 10 g/l suspension concentration

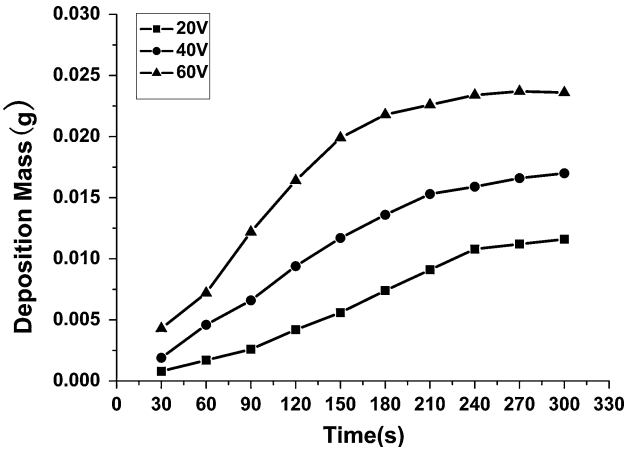

Fig. 4 Deposition masses at various deposition times under 20, 40, 60 V applied voltage

$$W = \int_{t_1}^{t_2} \mu \cdot E \cdot A \cdot C \cdot dt$$

where W, E, μ, A, C are the deposit amount, electric field strength, the electrophoretic mobility, the surface area of the electrode, the particle mass concentration in the suspension, respectively. Based on the Hamaker equation, while the solvent, the particles, and the apparatus for EPD are fixed, the weight of the deposited particles in the EPD method is a function of applied field, time and suspension concentration. As a result, the masses of the deposited particles and the thickness of the film can be readily controlled by the concentration of the suspension, applied voltage, and deposition time in the EPD method. In the present study, the suspension of glass–ceramic powders in ethanol, was positively charged and moved toward the cathode under the applied electric field.

Zhitomirsky, in his study on EPD of HA powders, indicated that under a constant voltage the coating thickness increased and the deposition rate decreased with deposition time [31]. Similar result was obtained in the present study. The deposition masses with increased and prolonged deposition time, under fixed applied electric fields of 20, 40, 60 V, are exhibited in Fig. 4. It illustrated that all the deposition rates (that is slope of the curves) under the app1ied voltage of 20, 40, 60 V decreased after a spell of deposition. In a constant voltage EPD, the result was expected because: While the potential between the electrodes was constant, the electric field intensity influencing electrophoresis was decreased by the formation of an insulating layer of ceramic particles on the electrode surface. That could be demonstrated by the decreased current with time, as reported in the literature [32]. Figure 5 illustrates the current behavior under different voltages during the EDP in a deposition time of 300 s under 20 V in 20 g/l suspension. The decrease of the current was caused by the increasing electrical resistance with the gradual depositing. In addition, the deposition masses and rates (that is slope of the curves) increased with the app1ied voltage changed from 20 to 60 V. According to the Hamaker equation mentioned above, the deposition rates

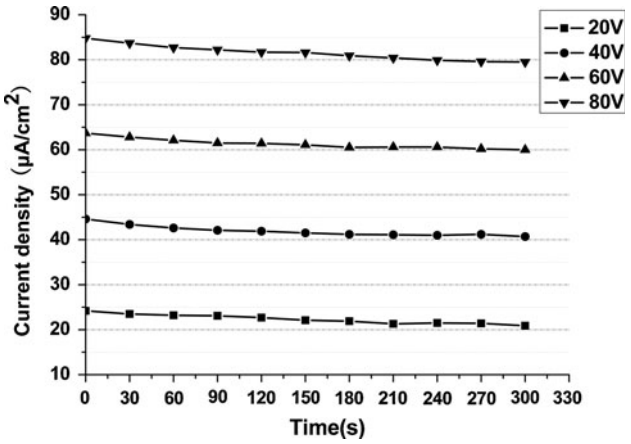

Fig. 5 Current behaviors under different voltages during the EDP in a deposition time of 300 s

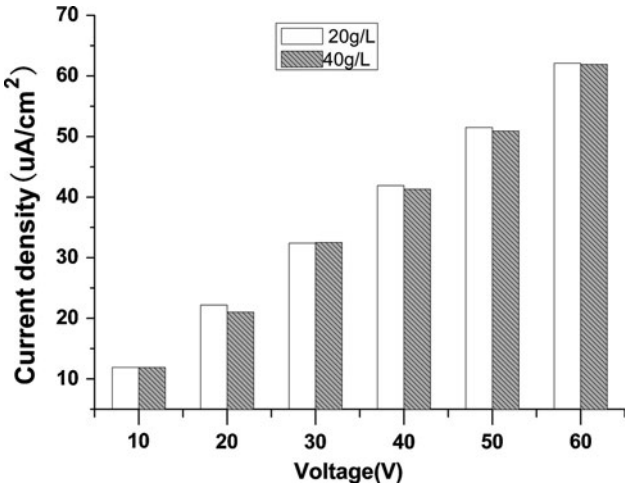

Fig. 6 Current densities of 20 and 40 g/l powder concentrations in solvents under different applied voltage

increased with the applied electric field strengths, when the other conditions were fixed.

The differences between 20 g/l and 40 g/l powder concentration upon the current did not reach statistical significance, as shown in Fig. 6. Because the electrical resistant of system was large and about 10^6 Ω, the changes of the electrical resistant caused by the changes of in the powder concentration were so small that the currents of different powder concentration suspensions were almost the same. The deposition weight increased with the concentration increase for the reason that there were more particles able to deposit on the substrates in per unit volume of suspension; accordingly, under the same electric field, it needed less deposition time to get the coatings with the same thickness in suspension of higher concentration than the lower one.

The SEM images of raw glass–ceramic coatings for 60 s, 120 s and 180 s, under 10 V voltage in 20 g/l suspension are displayed in Fig. 7. The deposited coatings showed more large particles and interspaces between the particles at the beginning 60 s. Then the smaller particles filled up the interspaces to form a thicker, more compact and homogeneous coating during the deposition progress.

The deposited coatings under different voltages possessed distinct deposition density and size distributions. It was observed that larger size particles were prone to deposit under the higher electric field, as shown in Fig. 8. The deposited coatings under 40 V, 60 V contained more large particles (>1 μm), whereas it was hardly found that large particles were deposited under 10 V and 20 V. Because higher voltage could offer great enough force to drive the agglomerated large particle motion. Correspondingly, the lower electric fields could drive only the smaller ones but not the large ones. It was also obvious that the coating of higher density and better uniformity was obtained under 10 V. Attributed to the lower deposition rate of the particles under 10 V, there was longer time to rearrange for particles, which resulted in a better density microstructure. The lower densities of coatings prepared under 20, 40, 60 V were ascribed to the shorter time rearrangement. In sum, 10 V was a most suitable voltage in virtue of the most impacted microstructure and less large particles.

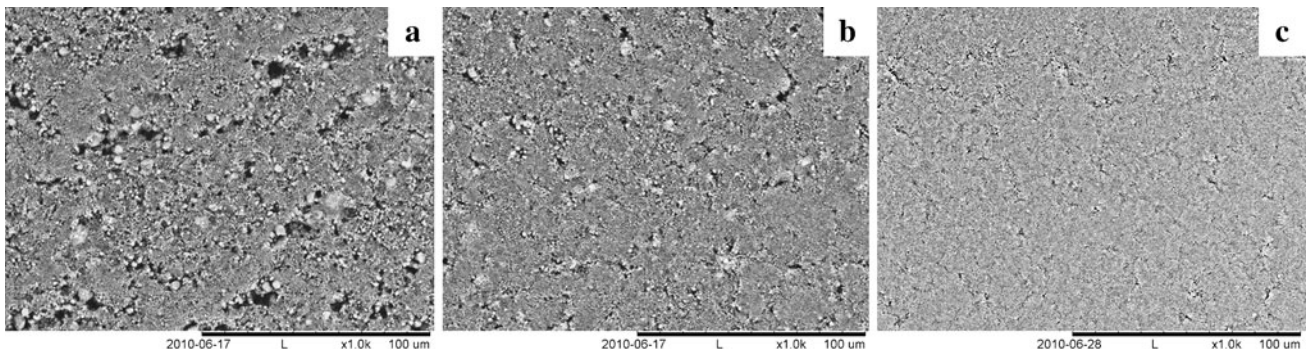

Fig. 7 SEM images of raw glass–ceramic coatings at different deposition time under 10 V voltage in 20 g/l suspension. **a** 60 s; **b** 120 s; **c** 180 s

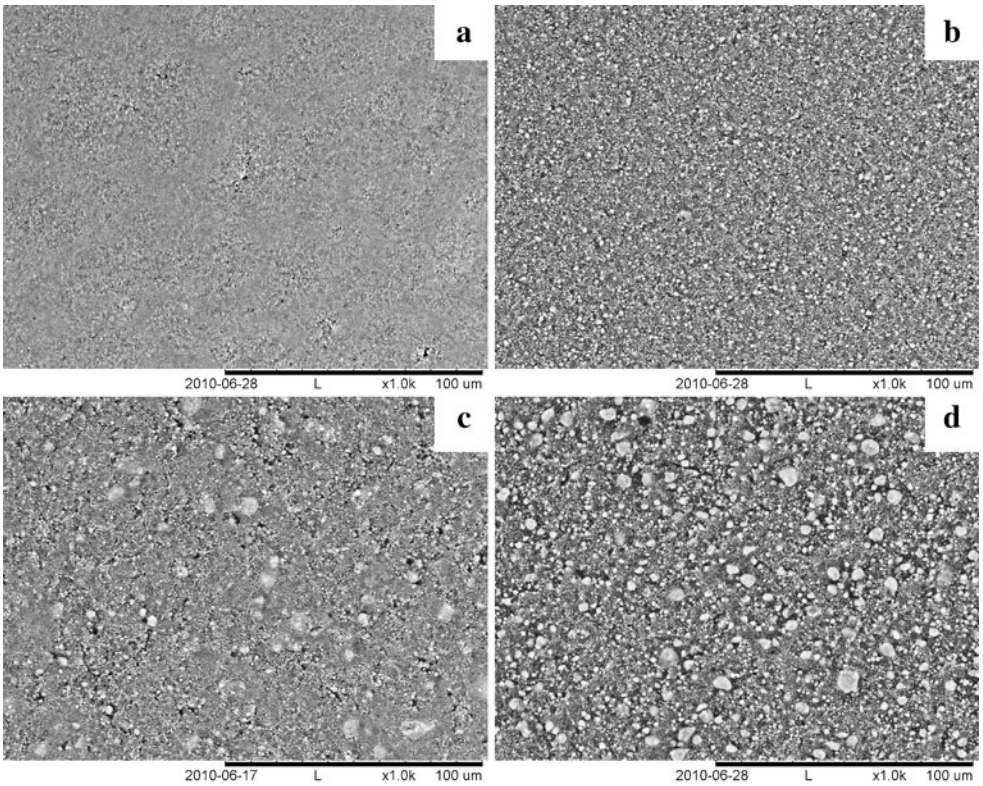

Fig. 8 SEM images of raw glass–ceramic coatings under different applied voltage. **a** 10 V; **b** 20 V; **c** 40 V; **d** 60 V

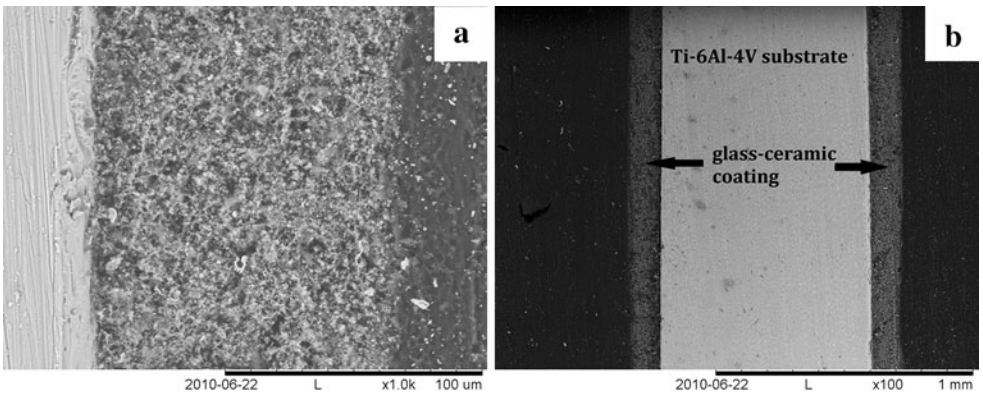

Fig. 9 SEM images showing the thickness of the coating, prepared under 80 V for 180 s in 40 g/l, at **a** high magnification; **b** low magnification

Thus, it could be concluded that the thickness and the density could be controlled by adjusting the suspension concentration, deposition time and applied voltage. Additionally, the glass–ceramic powders of the coatings were linked weakly but not chemically combined. Thus, heat treatment was necessary to strengthen the mechanical strength of the coatings and the bonding strength between the coatings and the substrates.

3.4 Characterization of the glass–ceramic coatings

The coatings with uniform thickness were achieved, and the thickness was approximately 10–150 μm, which could be controlled by the applied voltage, deposition time and concentration suspension. It was a potential method to prepare thick coatings. Figure 9 exhibits the cross section images of the relatively thicker coating that was about

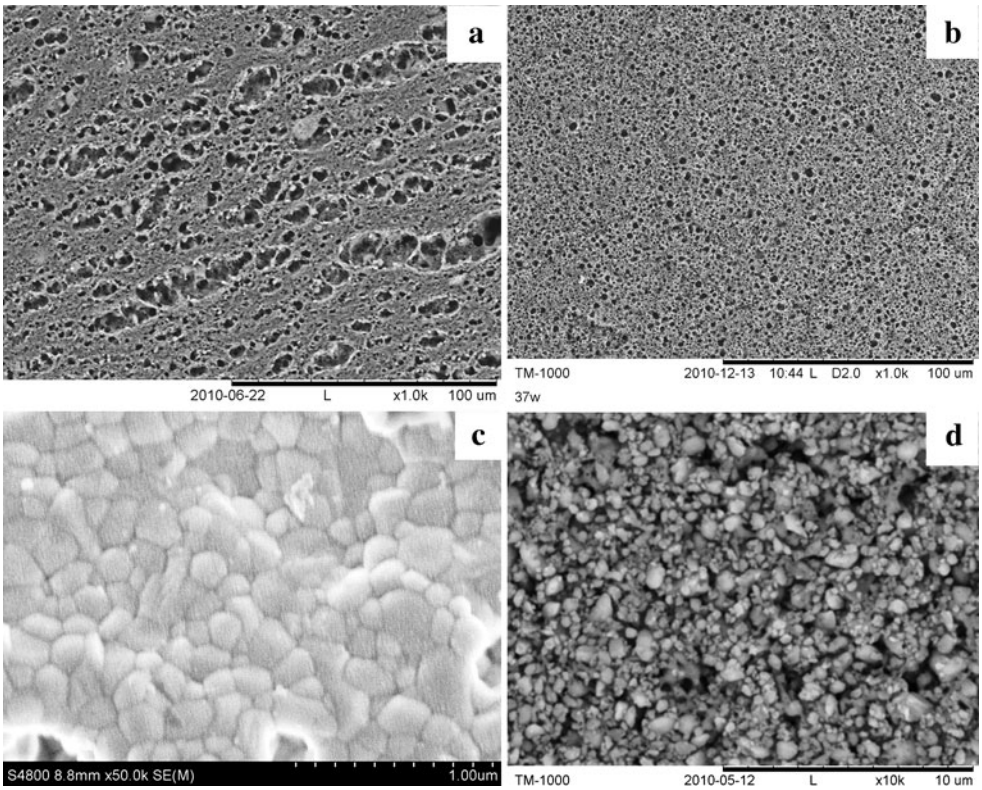

Fig. 10 SEM images of coating surfaces after calcined at 850°C for 3 h. **a** 10 V for 180 s in 20 g/l suspension; **b** 80 V for 180 s in 20 g/l suspension; **c** high magnification image of **b**; **d** without B_2O_3 additive

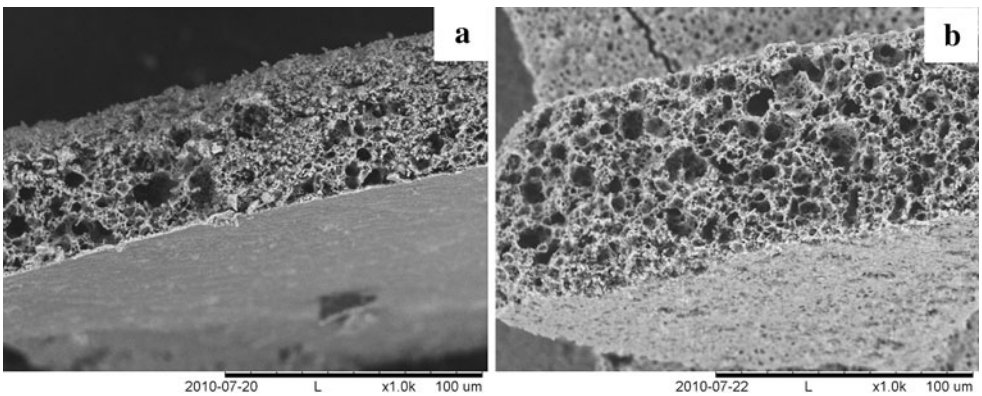

Fig. 11 SEM images of the profile of the glass–ceramic coatings calcined at 850°C. **a** 10 V for 180 s in 20 g/l suspension; **b** 80 V for 180 s in 20 g/l suspension

122 μm, deposited under 80 V for 180 s in 40 g/l suspension and calcined at 850°C for 3 h.

The microstructures of the coatings were porous of different morphologies as displayed in Fig. 10. Figure 10a shows the coating surface appearance of the coating prepared under 10 V applied voltage for 180 s in 20 g/l suspension. It possessed macropores with the diameter of approximately 10–20 μm and a large number of micropores. Figure 10b and c exhibit the coating surface morphology, containing more large particles, which was prepared under 80 V applied voltage for 180 s in 20 g/l suspension. Numerous micropores with the size of approximately 1–3 μm were uniformly sited on the crack-free coating surface. The porous ceramic structure, composed of grains with size of approximately 100–300 nm, formed by calcining the as-prepared coating at 850°C. It was attributed to the B_2O_3 additive helping to decrease the sintered temperature, while the coatings without the B_2O_3

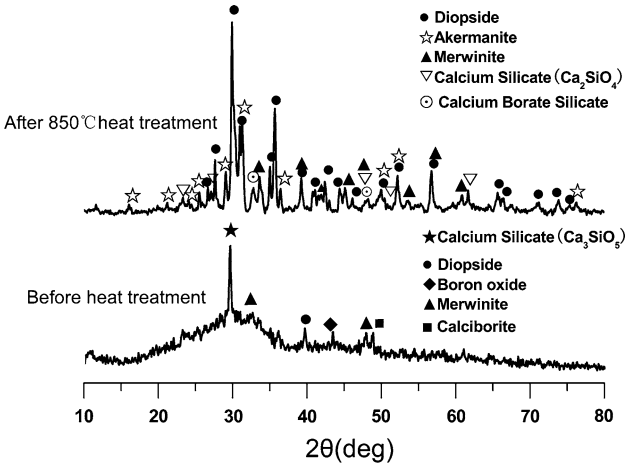

Fig. 12 XRD patterns of the coating before and after heat treatment

additive could not form ceramic coatings for its high sintered temperature as shown in Fig. 10d. Figure 11 shows the images of the profile of the coatings. It was observed that the coatings possessed a large number of interconnected pores, and the specimen prepared under 80 V (Fig. 11b) was looser than the one under 10 V (Fig. 11a). It hence could be deduced that EPD was a good processing method to form coatings with interconnected porous microstructure and desired thickness. The density and size distribution depended on the parameters of EPD, therefore, porous morphology could also be designed by appropriate control of the voltage, deposition time and suspension concentration. Researches indicated that the three dimensional cellular and porous structure could provide sufficient room for the transport of nutrients and cell growth, and thereby they were beneficial in osseous coalescence [25, 33–35]. The porous coatings were potential to be used as bioactive coatings.

The XRD patterns of the raw coating by EPD and the coating, prepared under 10 V for 180 s in 20 g/l suspension, and calcined at 850°C using a heating rate of 5°C/min are shown in Fig. 12. The coating after heat treatment was composed of multiphase ceramics and the main phases of the coating were diopside, akermanite, merwinite, calcium silicate and calcium borate silicate, which were different from the crystalline phases of the depositing powders calcined at 650°C. The main phases exhibited excellent bioactivity in the recent reports [8–13, 17–20]. The crystallinity of the coating heat-treated was approximately 92.6%, which was much higher than that of raw coatings. It was observed that diopside and akermanite were formed after heat treatment. The gel dried at 80°C for 24 h was characterized by TG and DSC as shown in Fig. 13. It could be deduced that the formation of the crystalline phases occurred at 779.5°C. In this study, the glass–ceramic porous coatings in CaO–Mg–SiO_2 system were prepared at the relatively low temperature, which was helpful to decrease the thermal stress and save energy. In addition, the good crystalline property of the coating might be beneficial for its stability in vivo [36].

Examination of apatite formation on the surface of a material in SBF was useful for predicting the bone bioactivity of the material in vivo [37]. Figure 14 shows the XRD pattern of the coating before and after immersion in SBF for 7 days. It indicated that bonelike apatite (JCPD 24-0033) was formed and the intensity of diopside, akermanite, merwinite, calcium silicate and calcium borate silicate peaks became weak after 7 days of soaking. The SEM micrographs of the coating surface soaked in SBF are exhibited in

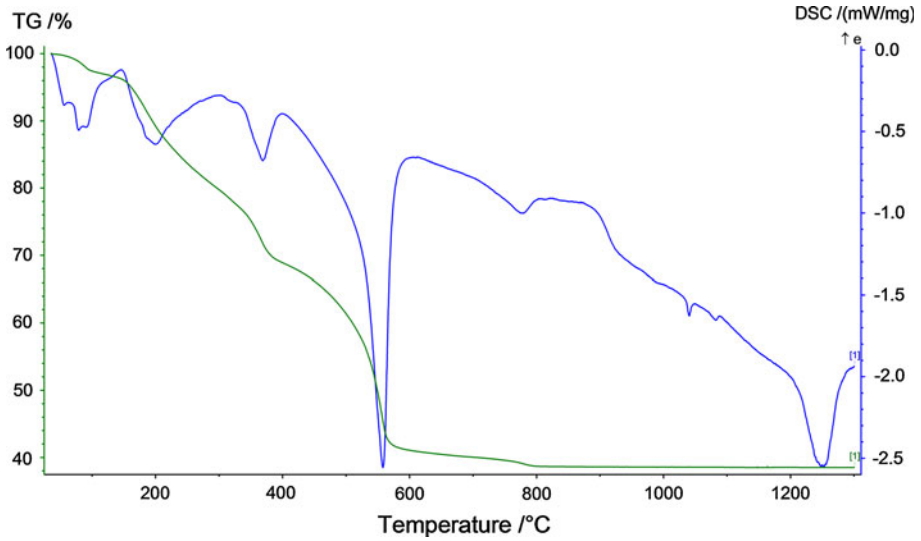

Fig. 13 TG and DSC curve of the dried gel

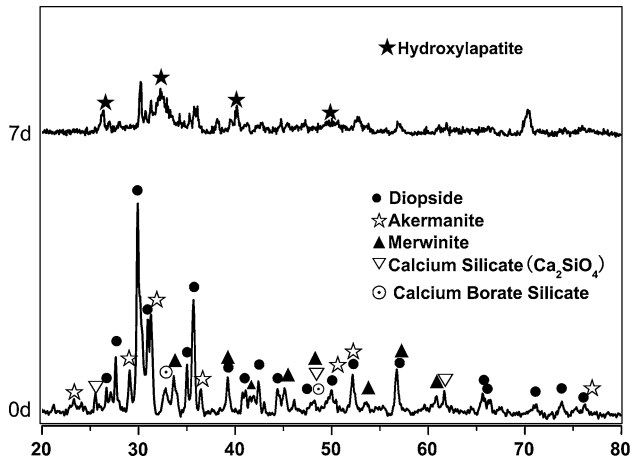

Fig. 14 XRD patterns of the coating before and after being soaked in SBF solution at 37°C for 7d

Fig. 15. The surface of the coating was a compact layer of spherical particles with diameters of about 2–4 μm, and the high-magnification micrograph showed that the particles were composed of claval crystallites, which were 40–60 nm in diameter and 300–600 nm in length.

Table 1 Bonding strengths of the coatings prepared in different conditions

Concentration (g/l)	Voltage (V)	Time (s)	Bond strength (MPa)
10	10	180	1.63
10	80	180	1.07
20	10	180	2.67
20	80	180	1.36
40	10	180	2.02
40	80	180	1.23

The bonding strength between coatings and substrates was in the range of 1.07–2.56 MPa, as shown in Table 1. The fracture surfaces of the coating prepared under 10 V for 180 s in 20 g/l suspension are shown in Fig. 16. It could be seen that the fracture occurred in the coatings, but not between the coatings and the substrates. The low bonding strength was attributed to the lower bonding strength between the particles in the coatings. In addition, the coatings prepared at 10 V for 180 s in 20 g/l suspension possessed the highest bonding strength for the reason

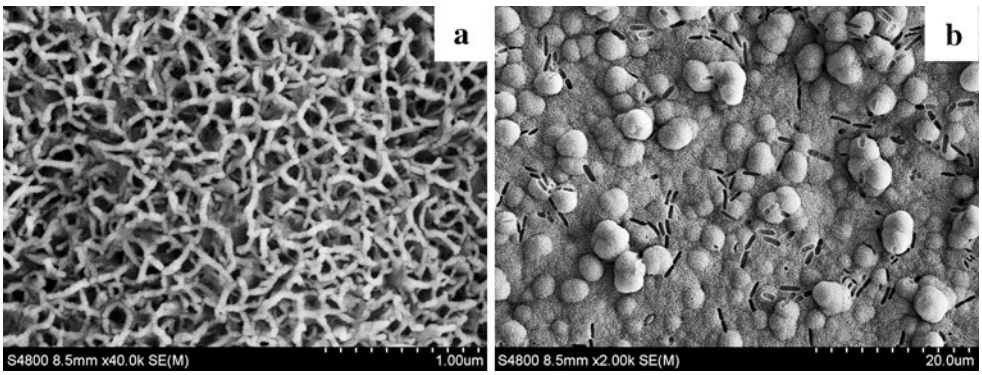

Fig. 15 SEM images of the coating after being soaked in SBF solution at 37°C for 7 d. **a** high magnification; **b** low magnification

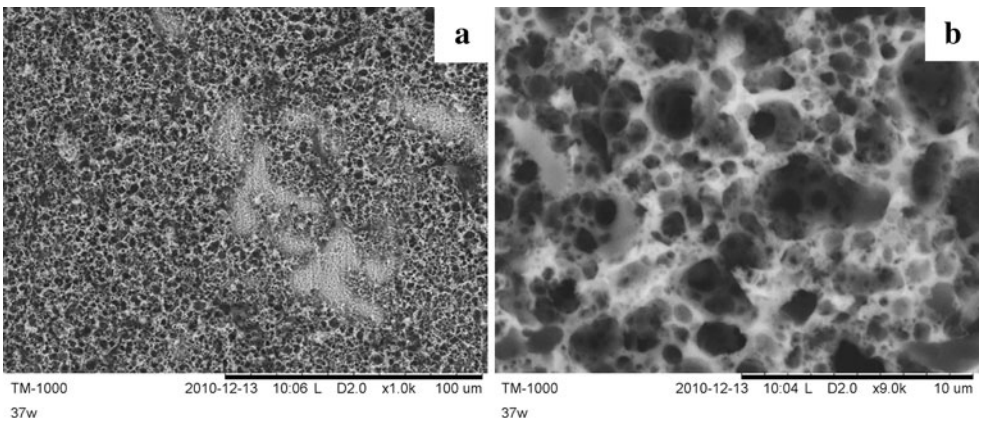

Fig. 16 SEM images of the fracture surfaces of the coating. **a** high magnification; **b** low magnification

that they were more compact than other specimens. Although the bonding strengths of the coatings were low, they could be improved by adjusting suspension system and parameters in EPD to be more impacted, and by optimizing heat treatment conditions in future.

4 Conclusions

The submicron CaO–MgO–SiO_2 glass–ceramic powders were prepared by sol–gel method. Ethanol was chosen to be the solvent of suspension system among five solvents. After being calcined at 850°C, uniform and crack-free porous CaO–MgO–SiO_2 glass–ceramic coatings with interconnected pore size of 1–20 μm were formed by EPD of submicron glass–ceramic powders. The pore appearances and porosity distribution could be controlled by adjusting the deposition time, applied voltage and the suspension concentration. The main phases of the coatings were diopside, akermanite, merwinite, calcium silicate and calcium borate silicate, which were high crystallinity after heat treatment. The bonding strength was low because the weak bonding strength between particles in the porous coatings resulted in the fracture, which needed improvement by optimizing the conditions of EPD and heat treatment conditions in future. In addition, bonelike apatite was formed on the coatings after being soaked in SBF, indicating potential bioactivity. Further research was also necessary to find the influence of different pore morphology, pore and its size distribution on the mechanical properties and the cell growth.

References

1. Zheng X, Huang M, Ding C. Bond strength of plasma-sprayed hydroxyapatite/Ti composite coatings. Biomaterials. 2000;21: 841–9.
2. Tomaszek R, Pawlowski L, Gengembre L, Laureyns J, Maguer AL. Microstructure of suspension plasma sprayed multilayer coatings of Hydroxyapatite and titanium oxide. Surf Coat Tech. 2007;201:7432–40.
3. Xu JL, Khor KA. Chemical analysis of silica doped hydroxyapatite biomaterials consolidated by a spark plasma sintering method. J Inorg Biochem. 2007;101:187–95.
4. Ma J, Wang C, Peng KW. Electrophoretic deposition of porous hydroxyapatite scaffold. Biomaterials. 2003;24:3505–10.
5. Cofino B, Fogarassy P, Millet P, Lodini A. Thermal residual stresses near the interface between plasma-sprayed hydroxyapatite coating and titanium substrate: finite element analysis and synchrotron radiation measurements. J Biomed Mater Res A. 2004;70(1):20–7.
6. Siriphannon P, Kameshima Y, Yasumori A, Okadaa K, Hayashi S. Formation of hydroxyapatite on $CaSiO_3$ powders in simulated body fluid. J Eur Ceram Soc. 2002;22:511–20.
7. Liu X, Ding C, Chu P. Mechanism of apatite formation on wollastonite coatings in simulated body fluids. Biomaterials. 2004;25:1755–61.
8. Ou J, Yin G, Zhou D, Chen X, Yao Y, Yang W, Wu B, Xue M, Cui J, Zhu H, Kang Y. Preparation of merwinite with apatite-forming ability by sol-gel process. Key Eng Mater. 2007;67: 330–2.
9. Wu C, Chang J, Ni S, Wang J. In vitro bioactivity of akermanite ceramics. J Biomed Mater Res. 2006;76A:73–80.
10. Nonami T, Tsutaumi S. Study of diopside ceramics for biomaterials. J Mater Sci: Mater Med. 1999;10:475–9.
11. Liu X, Tao S, Ding C. Bioactivity of plasma sprayed dicalcium silicate coatings. Biomaterials. 2002;23:963–8.
12. Sun H, Wu C, Dai K, Chang J, Tang T. Proliferation and osteoblastic differentiation of human bone marrow-derived stromal cells on akermanite-bioactive ceramics. Biomaterials. 2006; 27:5651–7.
13. Gil-Albarova J, Salinasb AJ, Bueno-Lozanoc AL, Roman J, Aldini-Nicolod N, et al. The in vivo behaviour of a sol–gel glass and a glass-ceramic during critical diaphyseal bone defects healing. Biomaterials. 2005;26:4374–82.
14. Xue W, Liu X, Zheng X, Ding C. Plasma-sprayed diopside coatings for biomedical applications. Surf Coat Tech. 2004;185: 340–5.
15. Wei M, Ruys AJ, Milthorpe BK, Sorrell CC. Electrophoretic deposition of Hydroxyapatite coatings on metal substrates: a nanoparticulate dual-coating approach. J Sol-Gel Sci Tech. 2001; 21:39–48.
16. Chen X, Ou J, Kang Y, Huang Z, Zhu H, Yin G, Wen H. Synthesis and characteristics of monticellite bioactive ceramic. J Mater Sci: Mater Med. 2008;19:1257–63.
17. Chen X, Wei Y, Huang Z, Kang Y, Yin G. Synthesis and characterization of multiphase bioactive glass-ceramics in the CaO–MgO–SiO_2 system with B_2O_3 additive. J Mater Res. 2008;23: 2873–9.
18. Ou J, Kang Y, Huang Z, Chen X, Wu J, Xiao R, Yin G. Preparation and in vitro bioactivity of novel merwinite ceramic. Biomed Mater. 2008;3:1–8.
19. Liu X, Marco M, Angelo C, Li B. Bioactive calcium silicate ceramics and coatings. Biomed Pharmacother. 2008;62:526–9.
20. Laxmidhar B, Liu M. A review on fundamentals and applications of electrophoretic deposition (EPD). Prog Mater Sci. 2007;52:1–61.
21. Lopez-Esteban S, Gutierrez-Gonzalez CF, Gremillard L, Saiz E, Tomsia AP. Interfaces in graded coatings on titanium-based implants. J Biomed Mater Res. 2009;88A:1010–21.
22. Wu C, Ramaswamy Y, Gale D, Yang W, Xiao K, Zhang L, Yin Y, Zreiqat H. Novel sphene coatings on Ti–6Al–4V for orthopedic implants using sol–gel method. Acta Biomater. 2008;4: 569–76.
23. Lin S, LeGeros RZ, LeGeros JP. Adherent octacalciumphosphate coating on titanium alloy using modulated electrochemical deposition method. J Biomed Mater Res. 2003;66(4):819–28.
24. Blackwood DJ, Seah KH. Influence of anodization on the adhesion of calcium phosphate coatings on titanium substrates. J Biomed Mater Res A. 2010;93:1551–6.
25. Wang C, Ma J, Cheng W, Zhang R. Thick hydroxyapatite coatings by electrophoretic deposition. Mater Lett. 2002;57:99–105.
26. Hayashi S, Konno K, Sugai M, Nakagawa Z. Electrophoretic deposition of $CaMgSi_2O_6$, fine powder prepared by coprecipitation method. J Mater Sci Lett. 2000;19:981–3.
27. Kokubo T. Surface chemistry of bioactive glass-ceramics. J Non-Cryst Solids. 1990;120:138–51.
28. Kolthoff IM, Bruckenstein S. Acid-base equilibria in glacial acetic acid. I. spectrophotometric determination of acid and base strengths and of some dissociation constants. J Am Chem Soc. 1956;78(1):1–9.

29. Negishi H, Yanagishita H, Yokokawa H. Proceedings of the electrochemical society on electrophoretic deposition: fundamentals and applications. In: Boccaccini.AR, editor. Receptor localization. New Jersey: Electrochemical Society; 2002. p. 216.
30. Hamaker HC. Formation of deposition by electrophoresis. Trans Farad Soc. 1940;36:279–83.
31. Zhitomirsky I. Electrophoretic hydroxyapatite coatings and fibers. Mater Lett. 2000;42:262–71.
32. Krause D, Thomas B, Leinenbachb C, Eifler D, Minaya EJ, Boccaccini AR. The electrophoretic deposition of bioglass particles on stainless steel and Nitinol substrates. Surf Coat Tech. 2006;200:4835–45.
33. Tachibana A, Furuta Y, Takeshima H, Tanabe T, Yamauchi K. Fabrication of wool keratin sponge scaffolds for lone-term cell cultivation. J Biotech. 2002;93:165–70.
34. Niklason LE. Engineering of bone graft. Nat Tech. 2000;18: 929–30.
35. Wintermantal E, Mayer J, Blum J, Eckert K-L, Luscher P, Mathey M. Tissue engineering scaffolds using superstructures. Biomaterials. 1996;17:83–91.
36. Fazan F, Marquis PM. Dissolution behavior of plasma-sprayed hydroxyapatite coatings. J Mater Sci: Mater Med. 2000;11:787–92.
37. Kokubo T, Takadama H. How useful is SBF in predicting in vivo bone bioactivity? Biomaterials. 2006;27:2907–15.